NORDIC VOLCANOLOGICAL INSTITUTE 79 03
UNIVERSITY OF ICELAND

RIFTING, MAGMATIC ACTIVITY AND INTERACTION BETWEEN ACID AND BASIC LIQUIDS

The 1875 Askja eruption in Iceland

by

Gudmundur E. Sigvaldason

Nordic Volcanological Institute
Reykjavik, Iceland

1979

NORDIC VOLCANOLOGICAL INSTITUTE 79 03
UNIVERSITY OF ICELAND

RIFTING, MAGMATIC ACTIVITY AND INTERACTION BETWEEN ACID AND BASIC LIQUIDS

The 1875 Askja eruption in Iceland

by

Gudmundur E. Sigvaldason

Nordic Volcanological Institute
Reykjavik, Iceland

1 9 7 9

CONTENT

ABSTRACT

Prior to the 1875 eruption of dacitic tephra in the Askja caldera in Northern Iceland basaltic magma was moved from deeper crustal levels to envelope a shallow dacite magma chamber. Heating of aquifers by the basaltic intrusion upset the hydrogeothermal system resulting in phreatic activity. Pressure release caused by a phreatic explosion initiated flash boiling and eruption of the dacite.

The intrusion of basaltic magma was associated with a rifting episode, which affected most of the 100 km long Dyngjufjöll fissure system. Basaltic magma, which accumulated beneath the floor of the Askja caldera intruded into the fissure system and some of it erupted 20 km to the south and 40 km to the north of the Askja caldera.

In situ mixing between basaltic and dacitic liquids was minimal. Deeper parts of the dacitic magma body had mixed incompletely with a small amount of basalt mainly on the contact zones between the two liquids. Mixing of basalt and the contents of the upper part of the dacitic magma chamber occurred in the eruptive channel. Slight heating of the dacite by the enveloping basalt resulted in loss of hydrogen from the dacitic magma and oxidation of the liquid.

INTRODUCTION

The Icelandic rift zone is a series of en echelon arranged fissure systems. The dimensions of the systems are variable, but typically 100 by 20 km in the northern part of the rift zone (Fig. 1). Each fissure system is volcanically active along its entire length, but the productivity of different sections is variable. One section, usually the central part of the system, is typically the most productive one, where rapid accumulation of volcanic rocks has resulted in a topographic high called a central volcano.

This paper is a study of a magmatic event on the Dyngjufjöll fissure system in the years 1874-1875. The event included both a plinian eruption of dacitic tephra and an eruption of basaltic lava. The eruption sites were separated by a distance of 40 km. Early students of the 1874-1875 events (Johnstrup, 1877; Lock, 1881; Thoroddsen, 1925) suggested that the two eruptions were somehow connected, but a definate indication as to the nature of this connection came first a century later, when a new magmatic event started on the adjoining Krafla fissure system (Fig. 1) (Björnsson et al., 1976, 1978; Tryggvason, 1978; Einarsson, 1978; Grönvold & Mäkipää, 1978). The magmatic event in Krafla is associated with rifting of a 60 km long section of the fissure system. Magma accumulates in a holding chamber at 3 km depth beneath the Krafla central volcano. Since December 1975 spasmodic rifting occurs at intervals of 3-5 months as magma from the holding chamber intrudes into the fissure system. Occasionally a splash of magma reaches the surface. The farthest distance magma has travelled in subsurface dykes during the Krafla event is 40 km, the same as the distance between eruption sites in the 1874-1875 event on the Dyngjufjöll fissure system.

The similarity between these events justifies the working hypothesis that the 1875 event was basically the same as the present Krafla event. The volcanological

aspects are, however, quite different, especially the production of acid tephra in the 1875 event.

THE GEOLOGY OF DYNGJUFJÖLL

The lowest exposed section in the Dyngjufjöll mountains are pillow lavas and hyaloclastites. All rocks are normally magnetized and probably much younger than 700.000 years. From about 650 m a.s.l. to 1500 meters height there is a continuous series of interlayered pillows and hyaloclastites. Subaerial lavas are conspicuously rare indicating that the major part of the visible topographic height above the surrounding is piled up beneath, or in close proximity to, an ice cap (Sigvaldason, 1968).

The Dyngjufjöll complex forms the central part of a fissure system. The dimensions of the system are 20 by 100 kilometers. The most productive part of the system where it passes through the Dyngjufjöll complex is 20 km long. This part of the fissure system is dominated by three caldera subsidences. The oldest of these calderas is relatively small and subsequently partly filled with basalt lavas. The second and major caldera cuts through the southern part of the previous subsidence. This caldera, Askja, is 7 km in diameter. Its age is probably less than 10.000 years, which is the time since massive retreat of glaciers of the last ice age. This age estimate for the Askja caldera is based on the absence of glacial erosion marks on the surface of lavas filling the first caldera, which in turn was cut by the Askja subsidence. The absence of recent hyaloclastites within the calderas suggests that permanent ice has not covered the area since the formation of the first caldera. The third caldera, the Askja lake, formed as a result of the 1874-1875 event.

The pattern of tectonic lineament (Fig. 2) within the fissure system can be divided into tow groups of alignments with slightly different strike. One NNE-SSW alignment is traceable from th edge of the Vatnajökull glacier in the south and disappears beneath postglacial lavas in the north of Dyngjufjöll. A second alignment with a more easterly trend starts in Dyngjufjöll and continues north across the basaltic shield volcano Kollóttadyngja. The caldera subsidences in Dyngjufjöll occurred at the intersection of these two alignments. After the second and major caldera subsidence the south end of the eastern alignment fanned towards west intersecting both calderas. At the same time the western fissure system became highly productive, especially along the western caldera wall. Lavas from these fissures flowed towards north and west from craters located outside the caldera. Lavas from craters inside the caldera have formed a thick (minimum 60 meters) layer on the caldera bottom. The filling of the caldera is controlled by an opening in its northeastern rim, where lavas poured out and spread over large areas to the east and south of Dyngjufjöll.

The recorded volcanic activity in Dyngjufjöll (1875 and later) has occurred within the Askja caldera on the curved southern end of the eastern fissure alignment and south of the caldera on a fissure, which trends through the caldera in the direction of the eastern alignment.

THE ERUPTION OF 1875

Historic record

Precursors to the eruption of 1875 were reported in February 1874. Unusually dense steamclouds were observed in Dyngjufjöll from afar. During the two last weeks of

December 1874 strong and frequent earthquakes were felt in North Iceland. On January 1st 1875 a column of smoke rose in direction south from the Mývatn district and on the following day frequent earthquakes were felt. On January 3rd fire was seen just east of due south from the Mývatn area, but cloudy weather obscured visibility soon afterwards. Earthquake activity came to an end a little later (Thoroddsen, 1925). From Eastern Iceland it was reported (Gunnarsson, 1875), that in the beginning of January 1875 two columns of smoke were seen in the direction of Dyngjufjöll. The distance between the columns was estimated in the order of 25 km. It can be safely assumed that one of these smoke columns came from Askja in Dyngjufjöll, which places the other one at the northern edge of Vatnajökull. If that activity was on the Dyngjufjöll fissure system, then this observation witnessed the formation of the lava field Holuhraun. On January 3rd 1875 tephra was reported to fall in NE Iceland (Fjallasveit and Kelduhverfi). Thoroddsen (1925, p. 217) reports that: "Nach eingeholten Erkundigungen im Jahre 1882 war diese Asche nicht liparitisch, sondern scheint eher basaltisch-palagonitisch zu sein". The Holuhraun crater row is partly covered by ice, which can account for the production of basaltic tephra.

On February 18th 1875 a basaltic fissure eruption started on Sveinagjá, 40 km north of Askja on the continuation of the Dyngjufjöll fissure system. This eruption lasted with short quiet intervals for several months and produced 0.2-0.3 km^3 of lava.

On February 15th 1875 four farmers from the Mývatn district visited Askja (Anonymous, 1875). They observed a subsidence in the SE corner of the caldera. An area of 3-4 hectares had subsided maximally 10 meters. To the west of the subsidence was an active crater, but the description indicates that no production of lava or tephra was ongoing, only violent boiling and mud pot activity. "Pumice and ash" had been deposited on the mountains to

the NE of the active area. The words "pumice and ash" in the farmers' terminology can mean deposits from a phreatic explosion without any juvenile material. The evidence for volcanic activity within the caldera at this time is therefore inconclusive. Comparison of the original descriptive text with observations of phreatic activity preceding the Askja eruption in 1961 and the presently ongoing activity at Krafla in Northern Iceland, favour the interpretation that only phreatic activity was occurring in Askja at the time of this visit.

Plinian outbreak started in the early morning of March 29th 1875. Tephra fell at 3:30 a.m. in Efri Jökuldalur 70 km to the east of Askja, carried by strong westerly winds. The tephra was greyish white in colour, fine grained and wet, so it could be formed like clay. This first phase lasted about one hour. At 5:30 in the morning the air had cleared somewhat, but shortly afterwards the main eruption started. Light brown pumice, with ever increasing grain size, rained down until noon. Although tephra fall stopped in populated areas, the eruption continued until in the morning of the following day. The tephra contained a number of white and black fragments of volcanic glass, as well as basaltic sand, which was much heavier than the pumice, and remained in place when everything else was removed by wind and water (Thoroddsen, 1925, p. 205).

In 1876 Askja was visited by the Danish geologist Johnstrup and his countryman the surveyor Caroc. This expedition described the scene of the eruption and made a map of the area (Johnstrup, 1877). They found a rounded triangular subsidence in the SE corner of the Askja caldera. It measured 4580 meters in E-W direction and about 2500 meters in N-S direction. The deepest part lay 232 meters below the floor of the caldera. At the bottom of the subsidence was a lake 1255 meters in diameter. Around the lake were numerous concentric faults, which had cut up the northern rim of the subsidence in a

steplike fashion. An informative observation made by this expedition was the occurrence of an obsidian dyke striking north-south along the eastern wall of the subsidence. This obsidian dyke had disappeared beneath water in 1884, when Askja was visited by Thoroddsen. At that time the lake level was 150 meters below the floor of the caldera (Thoroddsen, 1925, p. 215). The subsidence was practically filled with water to the present level in 1907, when studied by Spethman (1913).

Present field observations

The Askja lake is bounded to the south and east by precipitous hyaloclastite mountains and to the north and west by cliffs cutting the lavas, which cover the bottom of the Askja caldera (Fig. 3). The present level of the lake is 50 meters below the bottom of the caldera. soundings of the Askja lake reveal a roughly circular crater like depression with a maximum depth of 224 meters (Rist, 1975). Vigorous geothermal activity is manifest on the eastern and southern boarders of the lake and in wintertime small patches west of the central part of the lake remain ice free. A large crater, Víti, just NE of the subsidence, contains fumaroles and a small pond with warm water (30°C). This crater was long believed to be the main vent of the 1875 eruption in spite of early observations (Thoroddsen, 1925), which clearly show that this was not the case.

The volume of the lake is 1.231 km^3 and the area of the lake is 10.7 km^2 (Rist, 1975). The lake surface lies 50 m below the Askja caldera floor and the minimum volume above the lake surface is 0.54 km^3. However, the subsidence cuts the mountainsides to east and south of the lake, which are up to 400 m higher than the Askja caldera floor. It is therefore difficult to give an exact estimate of the total subsidence. The absolute minimum value is 1.77 km^3, but 2-2.5 km^3 is probably a more realistic figure.

The volume of the eruption products has been estimated by Thorarinsson (1944). The volume of freshly fallen tephra is 1.8 km^3 or 0.43 km^3 calculated as solid rock. The volume of the Sveinagjá lava is 0.2 to 0.3 km^3. A dyke going from Askja to Sveinagjá 1 km high and 4 m wide (Thorarinsson, 1968) has a volume of 0.16 km^3. Adding these figures together gives a total volume of known and implied material to leave a magma chamber beneath Askja of 0.89 km^3. This is less than half the volume of the subsidence.

The position of main vents and the succession of events can be pieced together by studying the distribution of the eruption products, which can be divided into groups according to physical appearance:

(1) Tephra ranging in colour and grain size from non vesicular greyish white, fine grained ash to vesicular pumice of light brown to black colour and with ever increasing grain size upward in the pumice deposit.

(2) Welded agglutinate, reddish to black in colour.

(3) Highly vesicular, black lava of the same chemical composition as the tephra.

(4) Less vesicular dykes of the same chemical composition as lava and tephra.

(5) Chunks of obsidián of various colour shades from black to greenish often partly vesiculated.

(6) Fragments of silicic rocks ranging from granophyre nodules to flint like angular glasses.

Of the presently visible eruption products the lava flow in the NE corner of the subsidence was the first to appear on the surface. A dyke along the eastern caldera fault is probably the feeder for the lava flow. Johnstrup (1877) observed a wall of obsidian parallel to the eastern fault. This dyke, which was later submerged, indicates that magma was intruded on a set of faults

along the eastern boundary of the caldera. The injection of the dykes and the formation of the lava flow belong definately to the 1875 event. This is evidenced by alteration of the tephra, which fell directly upon the lava surface. The tephra was altered to a claylike material, characteristic of intense alteration by hot acid solutions (Sigvaldason, 1959). This shows that the lava was still hot and degassing when covered by the tephra. The length of time between the emplacement of the lava and the deposition of the tephra can range from a few hours to several weeks.

The vent producing the lava is now concealed beneath a basaltic lava flow formed in 1923, but it is located roughly at a point, where the marginal dyke is cut by the main fissure of the 1875 eruption (Fig. 3). From craters on this fissure, which strikes in a ENE-SWS direction across the present Askja lake, came the bulk of the tephra produced in the plinian eruption. The first product was the nonvesicular greyish white, fine grained ash (Plate I). The distribution of this ash within the Askja caldera is shown in Fig. 4a. The prevailing strong westerly wind blew the material to the east. A layer (4-5 meters thick) of fine grained irregularily bedded ash was deposited on the east side of the vent or vents, but it thins out rapidly further east. On the windward side of the subsidence in the southwestern corner of the Askja caldera, the ash layer is maximally 3 meters thick, but thins out to zero within a few hundred meters from the 1875 subsidence. A sharp discontinuity in the tephra layer between the fine grained ash and the overlying brown to black pumice, represents the lull in activity from about 4:30 to 5:30 in the morning of March 29th 1875. This highly vesicular pumice was erupted with greater vigour, and a larger proportion of the material was carried outside the caldera than during the earlier phase. The distribution of material is distinctly different within the caldera (Fig. 4b).

A line drawn through the thickness maxima for the two phases indicates a parallel shift of the eruption fissure towards SE. Closing of the initial fissure due to subsidence may explain the pause in activity.

A pronounced difference is found between material deposited to the east of the subsidence and deposits on the windward side to the west. In the southwestern corner of the caldera the material, deposited directly on top of the greyish white ash from the first phase, is a welded agglutinate without any pumice material, neither at the top nor the bottom of the layer. The deposit has a restricted distribution, as shown in Fig. 3, and was most probably erupted from the southernmost vent on the fissure. It appears to be a counterpart to the lava flow at the other end of the fissure, except that the greater force of the eruption resulted in lava fountaining and the formation of a lava apron. After deposition the lava apron was hot enough to flow downhill as evidenced by slight folding of its surface. The similarity to lava aprons formed by basaltic lava fountains is striking, but not expected, in material of dacitic composition.

Towards the end of the eruption vents located close to the northeastern end of the fissure produced material hot enough to weld together into an agglutinate. This is covered by a layer of large pumice clasts, representing the waning phase of the eruption.

In a summary the sequence of events was as follows:

(1) Injection of dykes along the eastern caldera wall, which served as feeders to a dacitic lava flow.

(2) Opening of a ENE-WSW striking fissure(s) and production of fine grained ash for about one hour in a plinian eruption.

(3) The eruption stopped for about one hour before the main part of the plinian phase, which lasted for about 6 hours.

(4) The phreatic explosion crater Víti was formed after the plinian eruption came to an end.

The physical appearance of the eruption products is variable in spite of the fact that the chemical composition is uniform. The tephra is a mixture of dacitic and basaltic glasses, but the proportion of materials of contrasted compositions is variable and has no correlation with the differences in physical appearance (see section on petrology below). The difference in vesiculation can result from either or both of two effects. (1) Quenching of the liquid by contact with groundwater is supported by the observation that the pumice of the first phase was wet when deposited in Eastern Iceland. The shape of individual tephra grains furthermore indicates rapid chilling resulting in fractures resembling Surtseyjan type basaltic glasses (Walker et al., 1972). The discrete basaltic grains mixed with the tephra of the first phase are, however, not quenched, but form irregular rounded clots (Plate I). This can result from a two stage cooling of the basalt, first by mixing with the dacitic liquid resulting in consolidation to clots, and subsequently by contact with groundwater. (2) Secondly there is strong evidence for thermal layering of the magma chamber. The lava flow and the lava fountains produced at the extreme ends of the eruptive fissure indicate that lower viscosity of the dacite permitted nonexplosive extrusion. Lower viscosity at the same chemical composition results from higher temperature. If the eruptive fissure represents a diagonal cross section across the magma chamber, then the lateral parts were hotter than the center. If the tephra layer is an inverted vertical cross section through the magma chamber, then the welded agglutimate on top of the tephra sheet indicates that temperature in the chamber increased with depth.

PETROLOGY OF THE 1875 VOLCANIC PRODUCTS

The following description is based on samples taken at various levels in the thickest part of the tephra sheet cut by a fault in the NE wall of the 1875 subsidence (Fig. 5). Samples of silicic rock fragments erupted with the tephra were collected at various localities, both inside and outside the Askja caldera, but most of them were found in the vicinity of the crater Víti inside the caldera. Total analyses of bulk samples were done by standard methods of this laboratory (f.i. Imsland et al., 1977). Microprobe analyses were done by an ARL SEMQ fully automated crystal dispersive instrument. The petrological study was intended to reveal (1) the overall compositional character of the eruption products, (2) any compositional gradations, which could reflect processes within the magma reservoir prior to eruption, (3) the chemical and physical relation between the contrasting basaltic and dacitic liquids and (4) temperature distribution in the magma reservoir by studying mineral equilibria.

The tephra

Fig. 5 shows a section through the tephra layer in the northeastern corner of the Askja lake caldera and the position of samples taken. The first 4 meters are fine grained nonvesicular white tephra with irregular (base surge) bedding. This is overlain by 3 meters of coarser grained vesicular pumice of different colourshades between brown and black.

Bulk chemical analyses of the tephra samples are listed in Table 1. Microprobe analyses of glass fragments are listed in Tables 2 and 3. In spite of considerable search, no compositions intermediate between basalt and dacite were found. Mixing between the liquids did accordingly not result in chemical homogenization possibly

due to quenching of the basaltic component against the cooler dacite.

The microprobe glass analyses and the bulk chemical analyses can be used to calculate the modal amount of each component in the tephra (Table 4). The amount of basalt ranges from 0.4 to 14 per cent with a maximum amount at the bottom and top of the tephra sheet. It should be noted, that there is no correlation between the amount of the basaltic component and the colour of the tephra. On the contrary the tephra lightest in colour contains the highest amount of basalt.

In the nonvesicular ash the basaltic component occurs as distinct mechanically separable grains (Plate I). In the vesicular pumice the basaltic component is obscured, either by the very low amount or more intimate mixing. A textural relation showing intimate mixing between the two components is exemplified by a sample of obsidian (798) from the top of the tephra sheet. It contains an opaque basaltic and a colourless dacitic glass. Intermediate shades of translucent brown, produce a picture of turbulent mixing (Plate II). The apparent mixing between two glasses of contrasted composition is, however, not detectable by microprobe analyses. The colourless and brown glasses are identical in composition, while the opaque glass is a basalt (Tables 2 and 3). There can be no doubt, however, that the brown coloration of the acid glass is derived from contact with the basaltic component. The contaminant causing the coloration has either been added in such low concentration, that it cannot be detected by microprobe spot analyses, or is not included in the analyses program. The brown colour of the glass in the obsidian fragment, and the change in colour from grey to brown of the tephra at the beginning of the second phase of the plinian eruption, probably have the same cause.

It is indicative that the Fe_2O_3/FeO ratio in the tephra increases drastically at the beginning of the second phase of the eruption (Table 1, Fig. 5). This logically explains the colour change, but requires a process, which

would effectively and systematically influence the oxygen buffer of the magma reservoir.

It is assumed that the oxydation state of the tephra is inherited from a stationary magma with an initially homogenous oxygen fugacity. The liquid, its coexisting minerals and volatile components form a buffer sensitive to temperature changes and differential mass transfer. Small changes in temperature will not substantially alter the oxygen fugacity. Slight heating of the liquid can, however, alter the distribution of volatiles and result in differential diffusion. Oxydation of the liquid in the lower part of the magma chamber can result from the loss of hydrogen, in a way similar to the process suggested by Sato & Wright (1966) to explain the dramatic increase in oxygen fugacity in a drill hole into the Makaopuhi lava lake on Hawaii.

In Askja, during the 1875 event, the hydrogen fluxing was caused by heating of the magma by an external source. Hydrogen released from the lower part of the magma chamber was carried up through the dacitic liquid causing more water to dissociate and increasing the oxygen fugacity. The roof contact acted as a constriction to the hydrogen flux resulting in a build up of hydrogen in the uppermost part of the chamber, recombination of hydrogen and oxygen to water, and a drastic lowering of the oxygen fugacity (Fe_2O_3/FeO ratio of sample V1 is 0.03) in a narrow contact zone. The redistribution and loss of hydrogen from the magma chamber seems to adequately explain the colour change of the tephra.

Feldspars of the tephra

The composition of feldspars is about An 50 (oligoclase) in the bulk of the tephra (Table 5). The initial product of the plinian phase (top of the magma chamber) contains two feldspars, one similar to later feldspars, but slightly displaced towards lower An contents and an

anorthoclase similar to the feldspar phase of silicic rock fragments (see below). The obsidian (798) contains an oligoclase identical to the tephra feldspar and a bytownite from the admixed basalt.

The relation between feldspar and glass is shown graphically in the Ab-Or-An diagram (Fig. 6), where the normative composition of the liquid is plotted together with the feldspar composition. The compositional range is small, but there is a remarkable correspondence between liquid and solid compositions indicating that small variations in the liquid composition is reflected in the feldspar. The only exception is the sample from the bottom of the tephra sheet (V1), where the crystal liquid tie line has a different slope. The liquid composition lies well within the plagioclase volume of the feldspar-quartz tetrahedron. Projected on the SiO_2-Ab-Or base the normative composition of the liquid falls on the quartz side of the minimum melt composition at 2000 kb water pressure and about 6% An (Platen, 1965). The absence of quartz indicates that the crystallization of plagioclase occurred at considerably lower P_{H_2O} than 2000 bars.

It is informative that the slope of the tie lines between liquid and plagioclase in Fig. 6 is almost identical with the slope of tie lines between plagioclase and liquid in some hypersthene rhyolites from the Taupo volcanic zone in New Zealand (Ewart, 1969). It was noted by Ewart (1969) that plagioclase liquid tie lines in the system Ab-Or-An differed significantly with the type of coexisting ferromagnesian silicate. This was considered to reflect the decreasing crystallization temperature of the ferromagnesian silicate in the sequence hypersthene → hornblende → biotite.

The occurrence of similar coexisting hypersthene--plagioclase pairs in the Askja dacite and some Taupo rhyolites can be taken as supporting evidence for equilibrium between liquid and crystals.

The evidence for equilibrium gives increased conficence in the use of the plagioclase thermometer of

Kudo & Weill (1970). Table 4 lists the calculated temperatures for 0, 500, 1000 and 5000 bars water pressure. The temperature ranges from 891 to 978°C at 500 bars H_2O and 829 to 925°C at 1000 bars H_2O, which is comparable to the quenching temperatures found by Carmichael (1967) for salic volcanic rocks.

The pyroxenes of the tephra

Composition of coexisting calcium rich and calcium poor pyroxenes of the tephra are presented in Table 6 and shown graphically in Fig. 7. Both ortho and clinopyroxenes fall on the trend curves for pyroxenes in salic rocks (Carmichael, 1967), which are displaced towards the Di-Hd join and the Mg-Fe join relative to the Skaergaard trend. This displacement was suggested by Carmichael (1963) to result from lower crystallization temperature than that of the Skaergaard liquids.

Askja pyroxenes lie at the Mg-Di extreme of the trend curves similar to dacites from other volcanic areas (Ewart, 1971; Carmichael, 1967). This correspondence is a further support for chemical equilibrium between pyroxenes and liquid. There is apparently no correlation between temperature of crystallization and position of pyroxene on the trend curves. Carmichael (1967) determined the temperature indicated by iron titanium oxides in salic rocks containing hypersthene and obtained values in the range 895 to 980°C, which is the same range as indicated by the Kudo-Weill plagioclase thermometer at 500 bars H_2O for the Askja dacite.

The iron titanium oxides

High oxidation state of the dacitic magma is reflected in the iron titanium oxides. The lower, more reduced, part of the tephra layer contains unexolved magnetite, but

exolution is increasingly apparent from V5 upwards. Table 7 lists the analytical averages of titano magnetites and ilmenites, as well as the standard deviation from the mean. The pronounced increase in standard deviation in deeper parts of the magma chamber reflects the large compositional variation between individual grains due to the exolution. The average composition of oxides does, however, remain remarkably constant throughout the tephra layer.

The abrupt change in the Fe_2O_3/FeO ratio during the second part of the eruption is reflected in the exolution of titano-magnetite, but apparently the oxides have not come to equilibrium, probably due to constantly changing conditions. The evidence for a disequilibrium eliminates the possibility to use the oxide analyses for temperature determination on the basis of the experiments of Buddington & Lindsley (1964). The temperature indicated by the analyses ranges from 1100 to about 1150°C, which is evidently far outside reason. The useful information provided by the iron titanium oxides is therefore to confirm an unusually high oxidation state of the magma chamber, which can be explained by loss of hydrogen as detailed above.

The silicic rock fragments

Silicic rock fragments are abundant in the tephra sheet. Most common are flintlike angular pieces of various sizes and colour shades from white to grey.

One type has granophyric texture (794). Glass occurs in films and patches between grains of feldspar and quartz. Large specs of fine grained ore aggregate are associated with small ferroaugite grains. Zircon is a rare accessory. The texture indicates a state of partial fusion.

Another type (799) contains rounded quartz and mottled feldspar in a groundmass of glass with typical quench phases of tridymite, mullite and minor cordierite (Table 12).

A third type (800) is composed of a groundmass containing disseminated remnants of corroded quartz. Feldspar occurs in patches or groups of fine grained (few microns) individual idiomorphic crystals with optical continuity. The rock is veined with 0.1-0.5 mm quartz bands. Quench phases occur, but aluminium silicates are less conspicuous than in 799.

Table 8 contains bulk analyses of the silicic fragments. Groundmass analyses are listed in Table 9. There are some difficulties in equating the groundmass composition with the liquid phase. Due to sodium loss in these highly acid glasses, it was necessary to move the sample beneath the beam during analyses. This, combined with large amount of quench phases, prevents exact evaluation of modal compositions.

All rock fragments can be classified as plagidacite to rhyodacite according to the provisional classification attempt of Streckeisen (1976). This is, however, not without ambiguity since the somewhat unusual composition does not yield easily to standard classification schemes. By using the name dacite the normative orthoclase content and the An/Or ratio is given preference in the classification over normative quartz.

In spite of considerable textural variety the fragments are similar in chemical composition. Combined with obvious signs of variable degree of remelting it can be assumed that these silicic fragments are derived from the same unit of intrusive acid rock beneath the Askja caldera.

The feldspar of the granophyric dacite (794) (Table 10) is zoned from plagioclase to anorthoclase. Relicts of feldspars in extensively fused fragments are anorthoclases. All rocks contain free silica (quartz or tridymite). Minimum melts (in the sense used by Winkler, 1974) would be expected to have compositions approaching the cotectic line in the system Ab-Or-Qz-H_2O. Fig. 8 shows the position of bulk compositions of all analysed fragments

and respective liquid (groundmass) compositions of the granophyre (794) and two more extensively fused rocks (799, 800). Into the diagram is also drawn the trace of the cotectic line with numbers indicating the Ab/An ratios of bulk compositions producing respective "minimum melts" along the cotectic (Winkler, 1974), at 2 kb with excess water.

Both rocks (799, 800), which have fused extensively, have a groundmass composition, which falls close to the 2 kb cotectic at an Ab/An position matching closely the bulk ratio of the rocks. The liquid of fragment 794 falls farther away from the cotectic and on the opposite end of the line from that expected from the lower Ab/An bulk ratio. This is natural since the anorthite rich plagioclase of the granophyre is armored by anorthoclase and the effective Ab/An ratio controlling the composition of the intergranular liquid film will be high.

Those rock fragments, which are least affected by melting, are 792, 793 and 794 (granophyre). All others are depleted in iron, magnesium and calcium relative to these original compositions. The depletion goes hand in hand with peraluminous character, which probably results from removal of pyroxene (normative diopside), which is present in the granophyre, but absent in the corundum normative rocks. Those rocks, which are least affected by melting, are chemically identical to the tephra of the 1875 eruption.

It therefore appears safe to assume, that the fragments are derived from the consolidated margins of the reservoir containing the dacitic magma.

The basalt

Chemical analyses of basaltic glass from 3 tephra samples and the obsidian (798) are listed in Table 3. Analyses of basalts from the eruptions 1920-1961 (Table 2) are closely similar to the basalt of V1, V2 and 798, but the

basaltic glass of sample V3 is distinctly different. The V3 sample comes from a thin brown layer representing the initial product of the second part of the plinian phase (Fig. 5). The analyses of Table 3 is one of 11 identical analyses of different basalt fragments in this sample.

The discovery of this distinctly different basaltic liquid mixed with a small, but well defined, part of the tephra, puts a significant constraint on the mixing mechanism of the liquids.

The chemical composition of the basalt in V3 is previously unknown from the Dyngjufjöll complex. It is similar to basalts from the southern part of the Eastern Volcanic Zone of Iceland and similar basalts have been reported from the Kverkfjöll fissure swarm to the east of Dyngjufjöll (Sigvaldason, 1974, Table 1, No. 10). A discussion of the possible implication of such highly evolved basaltic liquids being available in the Dyngjufjöll area, is outside the scope of this paper, and will be treated elsewhere (Óskarsson et al., 1979).

Oxygen isotopes

Muehlenbacks et al. (1974) included a number of samples from the present study in their survey of oxygen isotopes ratios of Icelandic rocks. The δO^{18} values are listed in Table 8. The dacitic tephra has a very low δO^{18} value of +0.4 to +1.0 o/oo. The silicic rock fragments have a still lower ratio and display a large range in values from +1.0 to -9.9 o/oo.

The low δO^{18} value of the tephra can only be acquired by exchange with meteoric water, but diffusion in and out of a magma chamber at approximately 800 to 900°C is considered to be an unlikely process. The large amount of water required to bring the δO^{18} ratio from the normal value of +5.5 o/oo to +0.4 o/oo would have pronounced thermal effect on the magma, which is not evident in the phenocryst poor 1875 tephra. For reasons to be discussed

elsewhere (Óskarsson et al., in prep.) it is assumed that the dacitic liquid inherited the low δO^{18} value from its source.

The dacite was emplaced and started to crystallize at a depth, where groundwater could circulate in contact with the solidifying margins of the intrusion. Hydrothermal alteration is indicated by the quartz veins in some of the silicic fragments. The extremely low δO^{18} values are due to the low δO^{18} of the precipitation in the area[x)]. As a consequence of this interpretation the rock fragments with the lowest δO^{18} values are derived from the contact between the dacitic body and the wall rock, and the δO^{18} values would become progressively higher towards the solid-liquid interface. A comparison of texture and δO^{18} values in different silicic rock fragments shows a rough correlation. Those rock fragments, which are least affected by melting (794, 793, 792), have δO^{18} values of -5.2, -4.8 and +0.5 o/oo. Extensively melted rock fragments (1307, 800, 1200, 799) have δO^{18} values of -4.7, -7.4, -7.2 and -9.9 o/oo. This correlation indicates that the heat source effecting the melting of the solidified armour of the intrusion was more effective on the outside of that armour. This shows that the remelting of the already solidified dacite was not the result of reheating of the still liquid magma as might be the case if the dacite is mixed with a hotter basaltic liquid. On the contrary the dacitic magma reservoir was enveloped by the basaltic liquid, resulting in minimal mixing but some conductive heating of the dacitic liquid across the solidified granophyric armour.

x) The mean of four determinations of δ_D of surface waters in Dyngjufjöll is -93.45 o/oo (Árnason, 1976). The δO^{18} of the water is -12.93 o/oo according to the relation $\delta_D = 8\ \delta O^{18} + 10$ (Craig, 1961).

DISCUSSION

The 1875 eruption

Time relations: Emplacement of the dacitic magma body had occurred sufficiently long before the basalt to allow the contacts of the dacite to form an armour of granophyre. The solidified granophyre had exchanged oxygen isotopes with circulating ground water to such an extent, that the outermost shell had acquired an δO^{18} value close to that of the water. Since cooling rates and oxygen isotope exchange rates are unknown for this specific condition nothing can be said about the length of time between the emplacement of the dacite and the beginning of the rifting event.

The injection of basalt into a shallow crustal holding chamber is signalled by the increase in geothermal activity 13 months before the plinian outbreak. Since a part of the effect of the basaltic involvement in the event is that of melting the already solidified granophyre, the emplacement of the dacite precedes the basaltic intrusion probably by some years.

Space relations and the mixing of liquids: The simultaneous eruption of intimately mixed dacitic and basaltic liquids raises a question concerning the mixing process. The amount of basalt admixed to the dacitic tephra is greatest in the initial phase of the eruption (14%). When the main phase begins the amount of basalt has decreased (4%) and is now of a different composition. By the middle of the main phase the tephra is practically pure dacite, but towards the end basalt comes in again (9-12%), and is here of the same composition as in the initial phase. This pattern is incompatible with direct injection of basalt into the dacitic liquid and mixing by convection as suggested by Sparks & Sigurdsson (1977). Although the basalt may have intruded the dacitic magma locally, this did not result in pervase mixing. It

appears that the most significant spatial relation was that of the basaltic liquid enveloping the dacitic body. This is indicated by (1) the silicic rock fragments coming from the outermost shell of the solidified contact had suffered the most extensive melting and (2) the fact that dacite with high enough temperature to flow away from the vent as a lava or form a welded lava apron is erupted from the extremes of the fissure and also from the central part of the fissure towards the end of the eruption.

Mixing can have occurred on the contact zones between the two liquids aided by convection in the bottom section of the magma body, but not so at the sides or from the top.

A more effective mixing could have occurred during the eruption itself, as the dacite broke through a crustal layer, which was previously intruded by basalt. Such a process is indicated by the following arguments:

(1) Basaltic fragments occur as independent grains in the tephra of the first phase of the plinian eruption without compositional mixing or sintering together of the two different liquids. This suggests a quick succession of mixing and quenching.

(2) Phenocrysts (plagioclase and pyroxene) of the main bulk of the tephra are in equilibrium with the dacitic liquid. Admixture of up to 12% of basalt has not resulted in pronounced resorption of the phenocrysts, which should have occurred if chemical equilibrium was established between the two liquids at a higher temperature. Resorption of plagioclase is observed in material from the eastern extreme of the fissure.

Triggering of the eruption: Recently Sparks & Sigurdsson (1977) published a speculation on what might have triggered the 1875 eruption in Askja. They were aware that the eruption products were a mixture of a

silicic and a basaltic liquid and assumed that the basalt had intruded the silicic magma, mixed by convection, and both liquids then came to thermal equilibrium. The heating of the magma body by th˙s process would initiate boiling, build up pressure and finally lead to a plinian outbreak. Although the process of heating has been shown to be different from that visualized by Sparks & Sigurdsson (1977) the result might have been the same. However, the first portion of liquid to leave the magma chamber apparently made use of preexisting marginal faults of the Askja caldera. These established channels of escape do, however, not serve as release valves for the bulk of the dacitic magma, indicating that the magma chamber was not under a sufficient pressure to brake the flow resistance in the narrow marginal faults. The quiet outpouring of lava does on the contrary indicate a relatively low propelling energy during this first tapping of the magma chamber.

An alternative triggering mechanism is suggested by the intense phreatic activity observed in the caldera before and after the eruption. Phreatic activity associated with the 18th century rifting episode in the Krafla fissure system, can serve as an example of what might have happened in Askja on March 29th 1875. The Mývatn Fires 1724-1729 started with a violent phreatic explosion, which produced some juvenile material, both basaltic glass and granophyre in various stages of remelting. The production of fresh magmatic material shows that the explosion opened a path to a depth where magma was residing. In this case, however, the amount of available magma was not sufficient to sustain further production, but the crater remained active as a violent mud pot for more than a century. Such a phreatic explosion might have occurred in Askja. Here it so happened that a large body of a dacitic magma was available and ready to erupt provided that a sudden pressure release initiated flash boiling of the liquid.

ACKNOWLEDGEMENTS

Níels Óskarsson did most of the bulk chemical analysis, while Halldór Ólafsson assisted in the field. Edda Arnholtz typed the manuscript. I have profitted from discussions with all my colleagues at the Nordic Volcanological Institute. All this is gratefully acknowledged.

REFERENCES

Anonymus, 1875. Eldgosid, Ísafold 2: 35-37.

Árnason, B., 1976. Groundwater systems in Iceland traced by deuterium. Soc. Sci. Islandica 32: 1-236.

Björnsson, A., Saemundsson, K., Einarsson, P., Tryggvason, E. and Grönvold, K., 1977. Current rifting episode in North Iceland. Nature 266: 318-323.

Buddington, A.F. and Lindsley, D.H., 1964. Iron-titanium oxide minerals and synthetic equivalents. J. Petrol. 5: 310-357.

Carmichael, I.S.E., 1964. The petrology of Thingmúli, a Tertiary volcano in Eastern Iceland. J. Petrol. 5: 435-460.

Carmichael, I.S.E., 1967. The iron-titanium oxides of salic volcanic rocks and their associated ferromagnesian silicates. Contr. Min. Petrol. 14: 36-64.

Craig, H., 1961. Isotopic variations in meteoric waters. Science 133: 1702-1703.

Einarsson, P., 1978. S-wave shadows in the Krafla caldera in NE-Iceland, evidence for a magma chamber in the crust. Science Institute, RH-78-9 (mimeographed).

Ewart, A., 1969. Petrochemistry and feldspar crystallization in the silicic volcanic rocks, central North Island, New Zealand. Lithos 2: 371-388.

Grönvold, K., 1972. Structural and petrochemical studies in the Kerlingarfjöll region, central Iceland. Ph.D. thesis, University of Oxford.

Grönvold, K. and Mäkipää, H., 1978. Chemical composition of Krafla lavas 1975-1977. Nordic Volcanological Institute 7816 (mimeographed).

Gunnarsson, S., 1875. Vikuröskufall í Múlasýslum, 29. marz, 1875. Nordanfari 14: 58-59.

Helz, R.T., 1973. Phase relations of basalt in their melting range at P_{H_2O} = 5 kb as a function of oxygen fugacity. Part I. Mafic Phases. J. Petrol. 14: 249-302.

Helz, R.T., 1976. Phase relations of basalt in their melting range at P_{H_2O} = 5 kb. J. Petrol. 17: 139-193.

Imsland, P., 1978. The petrology of Iceland, some general remarks. Nordic Volcanological Institute 7808 (mimeographed).

Imsland, P., Larsen, J.G. Prestvik, T. and Sigmond E., 1977. The geology and petrology of Bouvetöya, South Atlantic Ocean. Lithos 10: 213-224.

Johnstrup, F., 1877. Om de 1875 forfaldne vulkanske Udbrud paa Island. Geografisk Tidsskrift 1: 50-66.

Kudo, A.M. and Weill, D.F., 1970. An igneous plagioclase thermometer. Contr. Min. Petrol. 25: 52-65.

Lock, W.G., 1881. Askja, Iceland's largest volcano. Charlton, Kent.

Mäkipää, H., 1978. Mineral equilibria, geothermometers and geobarometers in some Icelandic hyaloclastites. Bull. Geol. Soc. Finland 50: 113-134.

Muelenbachs, K., Anderson, A.T. and Sigvaldason, G.E., 1974. Low O^{18} basalts from Iceland. Geochim. Cosmochim. Acta 38: 577-588.

Óskarsson, N., 1978. Effect of magmatic activity on fumarole gas composition in the Námafjall-Krafla volcanic center, N-Iceland. Nordic Volcanological Institute 7803 (mimiographed).

Óskarsson, N., Sigvaldason, G.E. and Steinthórsson, S., 1979. A dynamic model of rift zone petrogenesis and the regional petrology of Iceland. Nordic Volcanological Institute 7905 (mimeographed).

Pálmason, G., 1967. On heat flow in Iceland in relation to the Mid-Atlantic Ridge. In: Iceland and Mid-Ocean Ridges (ed. S. Björnsson). Soc. Sci. Islandica 38: 111-127.

Platon, H.v., 1965. Kristallisation granitischer Schmelzen. Beitr. Mineral. u. Petrogr. 11: 334-381.

Rist, S., 1975. Stöduvötn. Orkustofnun, OS-Vatn 7503. Reykjavik.

Sato, M. and Wright, T.L., 1966. Oxygen fugacity directly measured in volcanic gases. Science 153: 1103-1105.

Sigvaldason, G.E., 1959. Mineralogische Untersuchungen über Gesteinszersetzung durch postvulkanische Aktivität in Island. Beitr. Mineral. u. Petrogr. 6: 405-426.

Sigvaldason, G.E., 1968. Structure and products of subaquatic volcanoes in Iceland. Contr. Mineral. Petrol. 18: 1-16.

Sigvaldason, G.E., 1974a. Basalts from the center of the assumed Icelandic mantle plume. J. Petrol. 15: 497-524.

Sigvaldason, G.E., 1974b. The petrology of Hekla and origin of silicic rocks in Iceland. In: The eruption of Hekla 1947-1948, Soc. Sci. Islandica 5: 1-44.

Sparks, S.R.J. and Sigurdsson, H., 1977. Magma mixing: a mechanism for triggering acid explosive eruptions. Nature 267: 315-318.

Spethman, H., 1913. Islands grösster Vulkan. Die Dyngjufjöll mit der Askja. Leipzig: 1-143.

Streckeisen, A., 1976. Classification of the common igneous rocks by means of their chemical composition. A provisional attempt. N. Jb. Miner. Mh. 1: 1-15.

Thorarinsson, S., 1944. Tefrokronologiska studier på Island. Geografiska Annaler 26: 1-217.

Thoroddsen, Th., 1925. Die Geschichte der isländischen Vulkane. Det kongelige Danske Videnskabernes Selskabs Skrifter 8, 9: 1-458.

Tryggvason, E., 1978. Tilt observations in the Krafla-Mývatn area 1976-1977. Nordic Volcanological Institute 7802 (mimeographed).

Walker, G.P.L., 1966. Acid volcanic rocks in Iceland. Bull. Volc. 29: 375-406.

Walker, G.P.L. and Croasdale, R., 1972. Characteristics of some basaltic pyroclastics. Bull. Volc. 35: 303-317.

Winkler, H.G.F., 1974. Petrogenesis of metamorphic rocks. Springer: 1-320.

Yoder, H.S., Jr., 1973. Contemporaneous basaltic and rhyolitic magmas. Am. Mineral. 58: 153-171.

TEXT TO FIGURES

Fig. 1. The fissure systems of the rift zone in North Iceland (after Björnsson et al., 1977).

Fig. 2. A geological map of the Askja area and southern part of the Dyngjufjöll fissure system. Only a small number of fissures and crater rows are shown on the map to indicate the strike of main tectonic lineaments.

Fig. 3. A map of the Askja caldera lake formed after the 1875 eruption, showing the distribution of lavas and agglutinates from the 1875 eruption and lavas of later volcanic events.
(1) Bátshraun, eruption 1921.
(2) N- and S-Botnahraun, 1923.
(3) Eruption of 1926.
(4) Mývetningahraun, 1922.

Fig. 4. Thickness of the 1875 tephra layer around the caldera lake.
A: White tephra of the first phase.
B: Brown to black tephra of the second phase.
(Numbers in centimeters).

Fig. 5. A cross section through the tephra layer at the NE corner of the caldera lake (see Fig. 3). V1 to V7 show location of samples taken (B = black; Br = brown). The cross hatched bottom layer is a dacitic lava. The variation in the Fe_2O_3/FeO ratio and wt.% H_2O is shown to the right.

Fig. 6. Composition of feldspars (crosses) and coexisting glasses. Numbers refer to samples V1 to V7 (Fig. 5).

Fig. 7. Composition of coexisting pyroxenes. The broken line is the pyroxene trend in the Skaergaard intrusion.

Fig. 8. Silicic rock fragments plotted in the qz, ab, or diagram. Open circles are bulk compositions and crosses are respective groundmass compositions. Points represent the composition of tephras. The minimum melt composition in the system at 2 kb and different Ab/An ratios (numbers) is shown by the line drawn through squares (Winkler, 1974).

TEXT TO PLATES

Pl. 1. a) Tephra of the first phase of the eruption. Black dot at bottom right is basalt.
b) Tephra of the second phase.

Pl. 2. Contact between dacite and basalt. Only the pitch black areas are basalt while all shades of translucent brown are pure dacite with differing Fe_2O_3/FeO ratios.

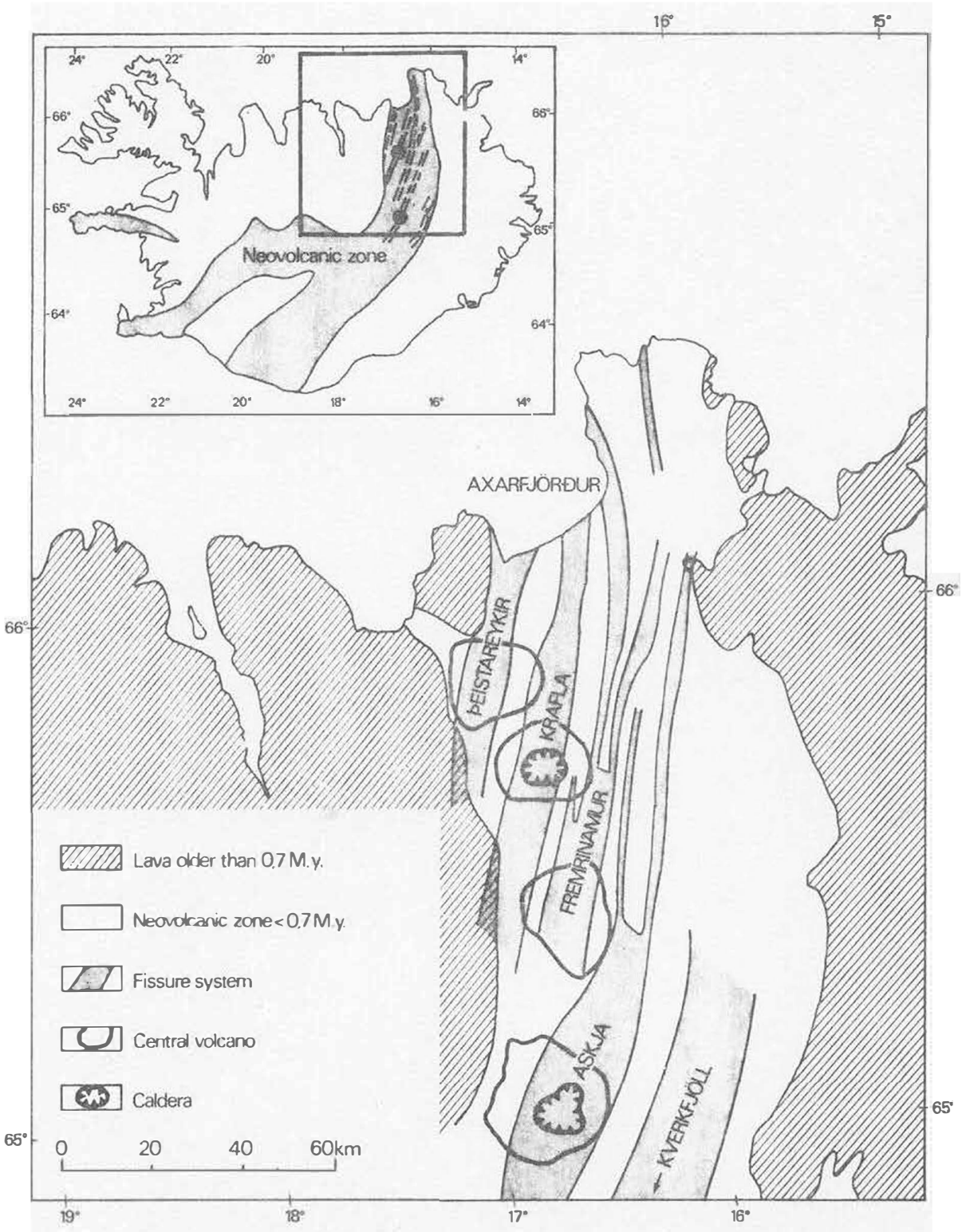
Neovolcanic zone
AXARFJÖRÐUR
ÞEISTAREYKIR
KRAFLA
FREMRINÁMUR
ASKJA
KVERKFJÖLL
Lava older than 0,7 M.y.
Neovolcanic zone < 0,7 M.y.
Fissure system
Central volcano
Caldera
0 20 40 60km

Fig. 1.

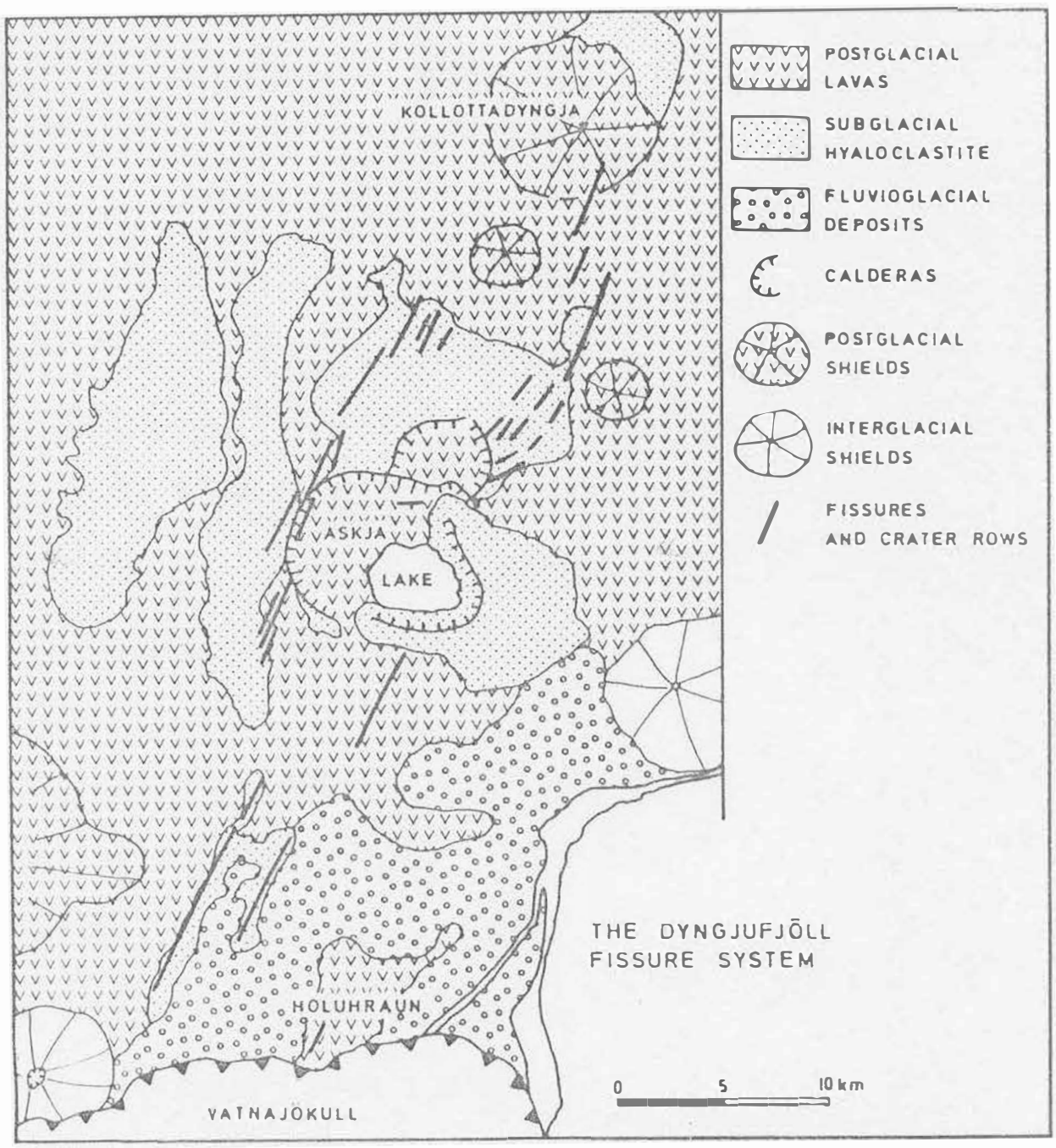
KOLLOTTADYNGJA
ASKJA
LAKE
HOLUHRAUN
VATNAJÖKULL
POSTGLACIAL LAVAS
SUBGLACIAL HYALOCLASTITE
FLUVIOGLACIAL DEPOSITS
CALDERAS
POSTGLACIAL SHIELDS
INTERGLACIAL SHIELDS
FISSURES AND CRATER ROWS
THE DYNGJUFJÖLL FISSURE SYSTEM
0
5
10 km

Fig. 2.

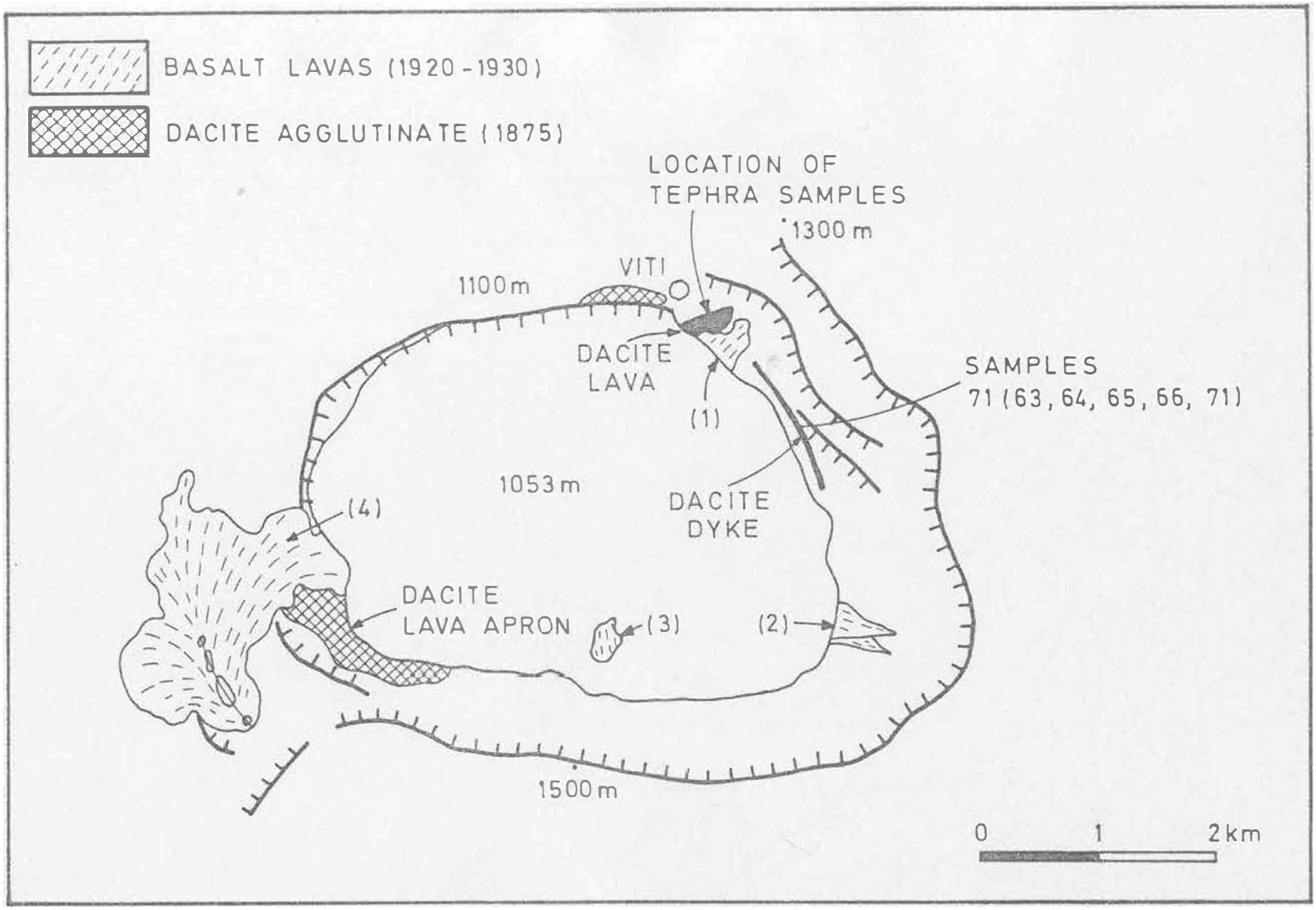
BASALT LAVAS (1920-1930)
DACITE AGGLUTINATE (1875)
LOCATION OF TEPHRA SAMPLES
1300 m
VITI
1100m
DACITE LAVA
(1)
SAMPLES 71 (63, 64, 65, 66, 71)
1053 m
DACITE DYKE
(4)
DACITE LAVA APRON
(3)
(2)
1500 m
0
1
2km

Fig. 3.

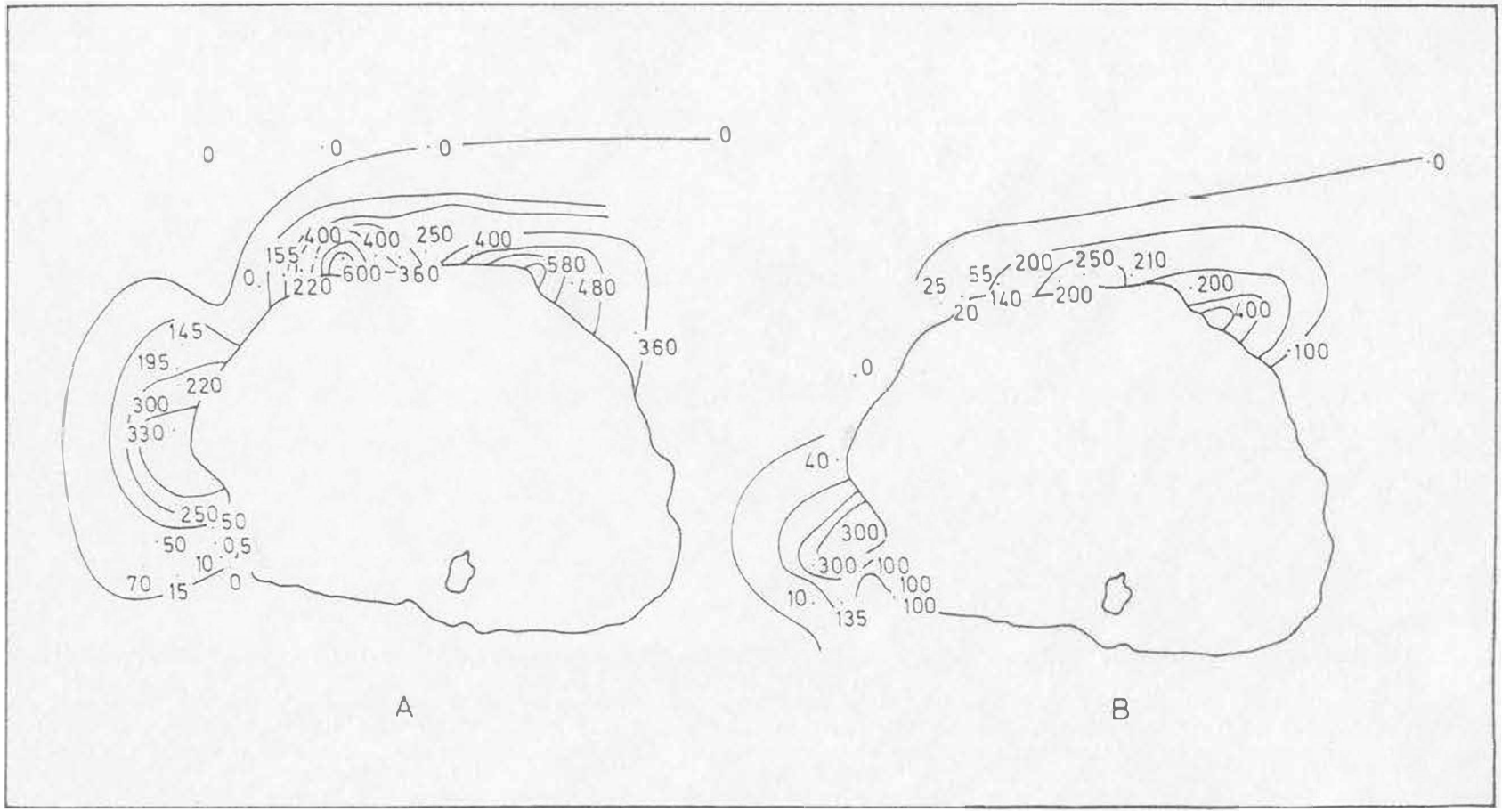
0
0
0
0
400
400
250
400
155
0
220
600
360
580
480
360
145
195
220
300
330
250
50
50
0,5
10
70
15
0
A
0
25
55
200
250
210
20
140
200
200
400
100
0
40
300
300
100
100
10
135
100
B

Fig. 4.

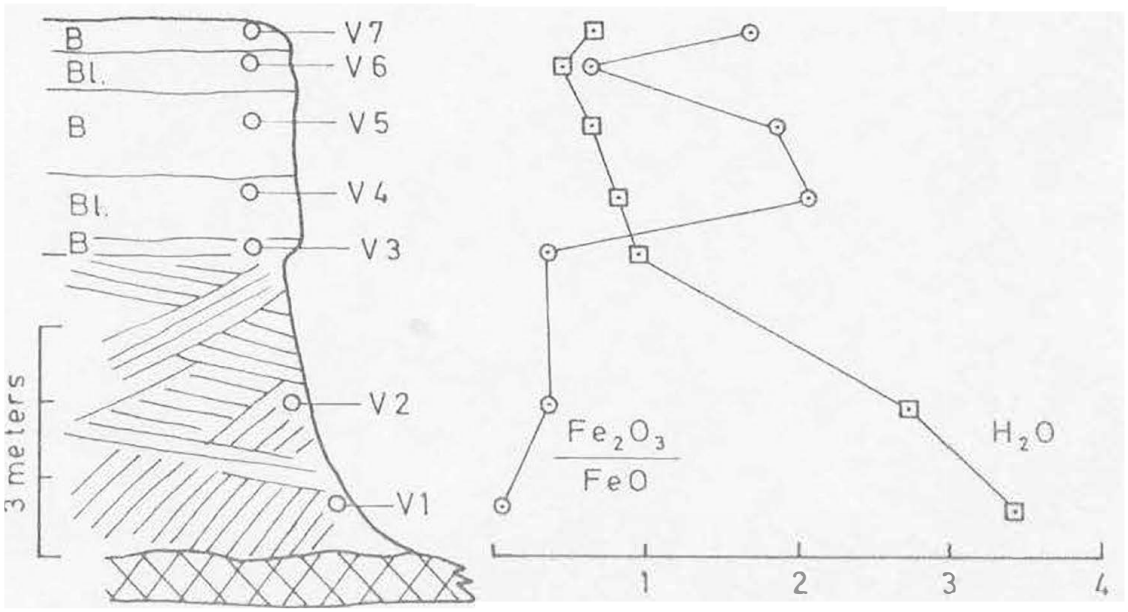

Fig. 5.

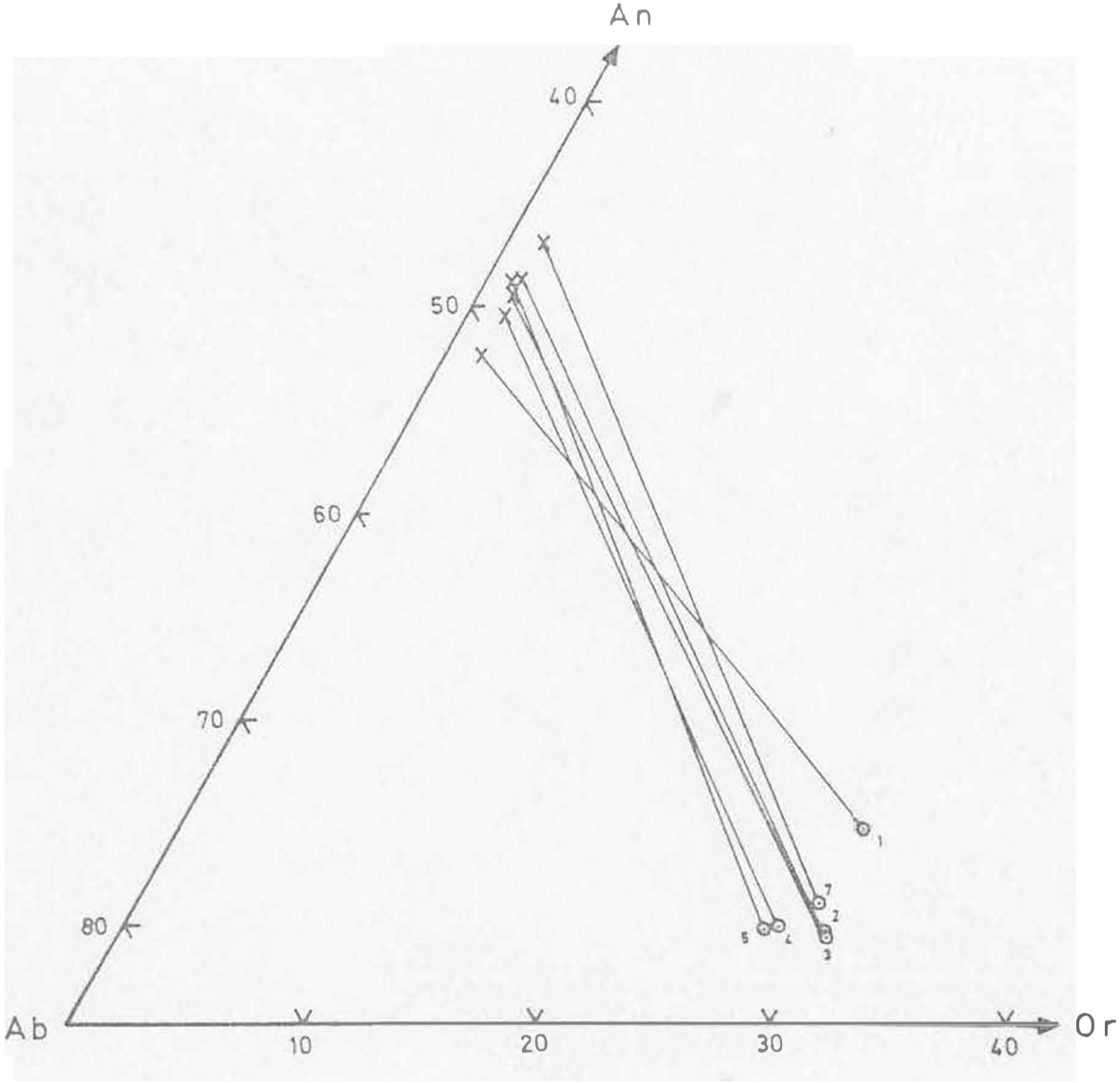

Fig. 6.

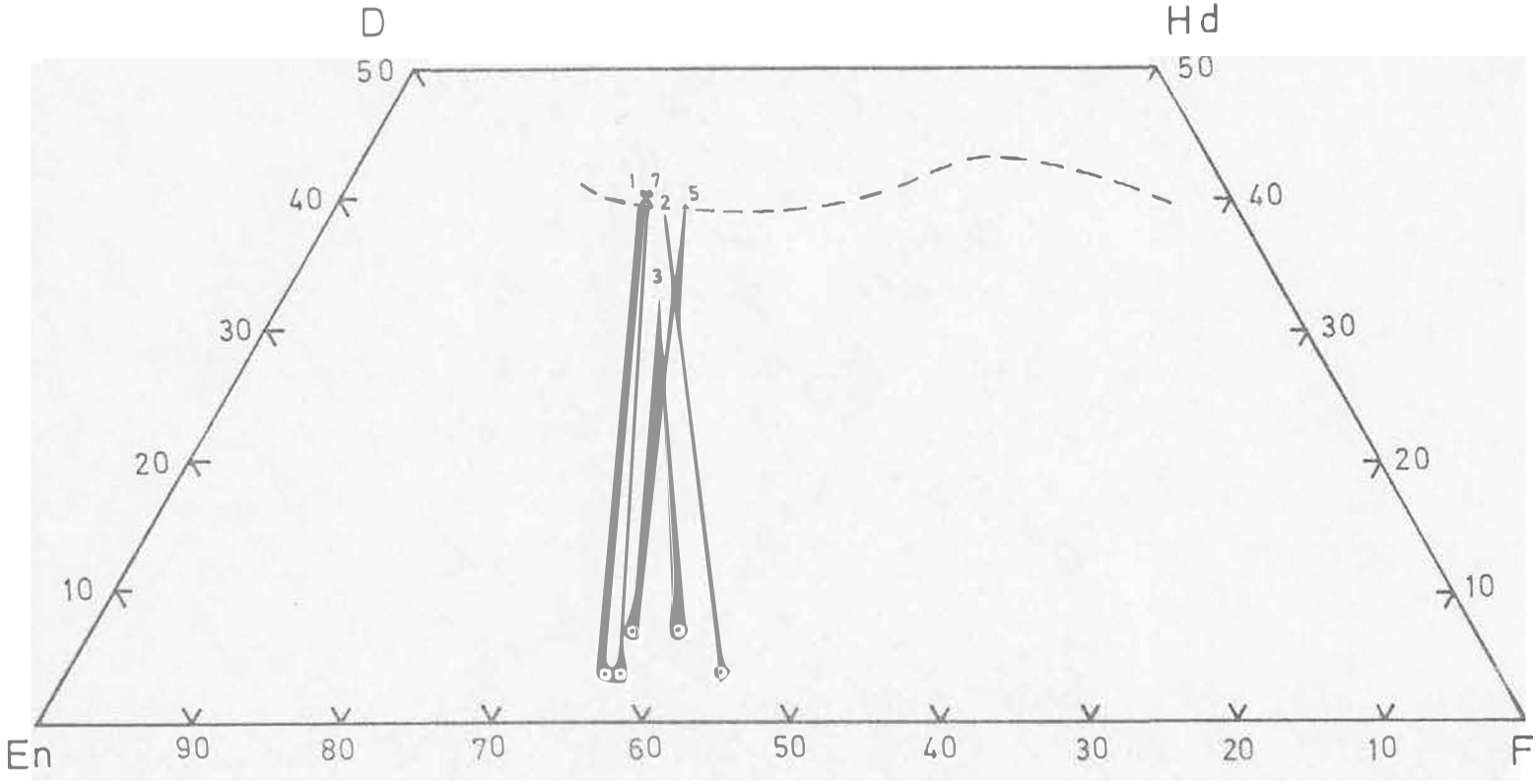
D
Hd
50
40
30
20
10
50
40
30
20
10
1
7
2
5
3
En
90
80
70
60
50
40
30
20
10
Fs

Fig. 7

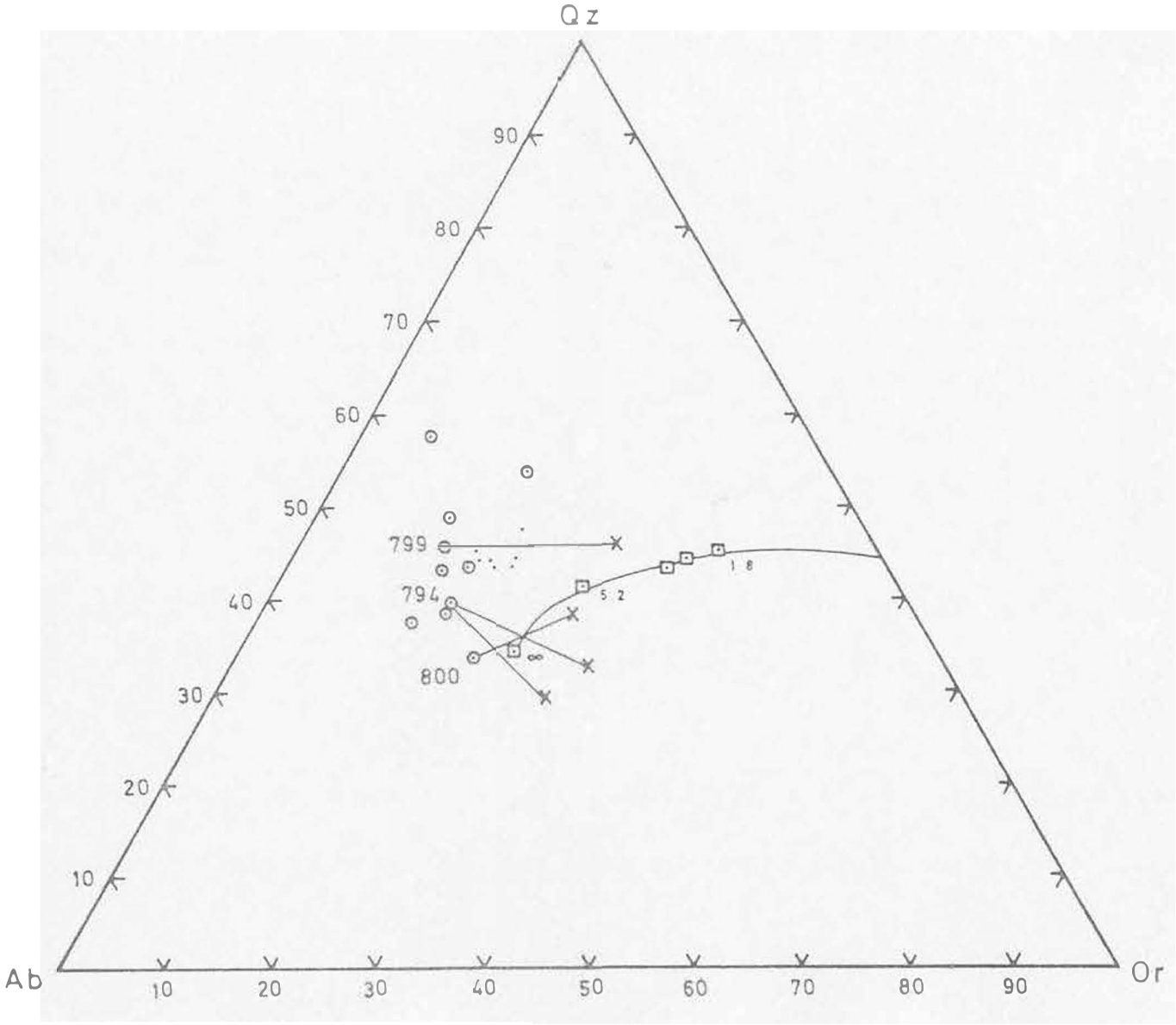

Fig. 8.

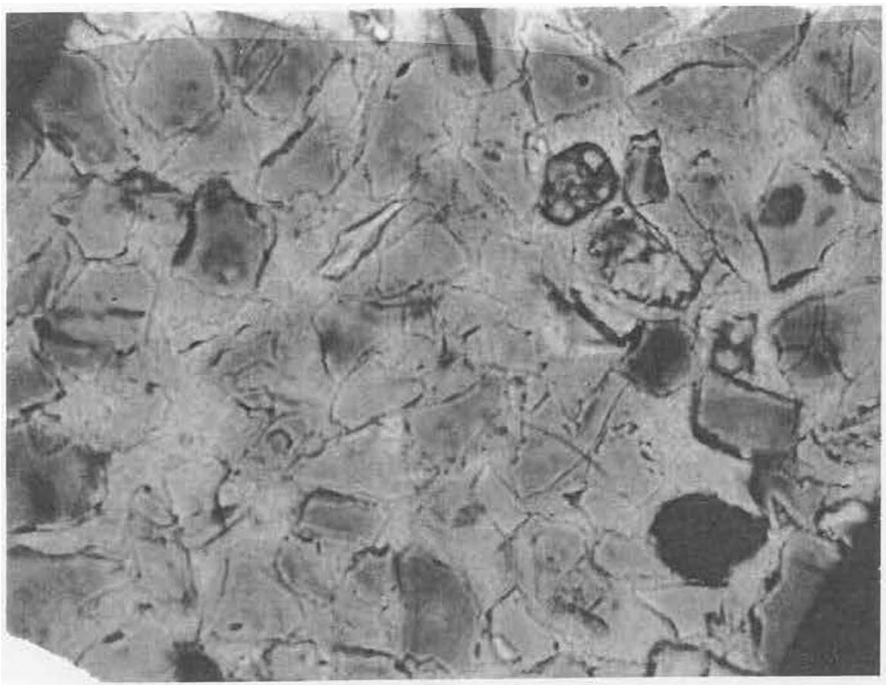

Plate Ia

Plate Ib

Plate II

TEXT TO TABLES

Table 1. Bulk chemical analysis (see Fig. 3 for sample location).

Table 2. Microprobe analysis of acid glasses.
798L = colorless glass from obsidian.
798B = brown glass from obsidian.
Number of individual analysis in paranthesis.

Table 3. Microprobe analysis of basaltic glass.

Table 4. Plagioclase temperatures (Kudo-Weill) °C.

Table 5. Feldspar analysis.

Table 6. Pyroxene analysis.

Table 7. Oxides in tephra. Number of individual analysis behind the average is given in parenthesis.
s = standard deviation.

Table 8. Bulk analysis of silicic rock fragments.

Table 9. Microprobe analysis of groundmass of silicic rock fragments.

Table 10. Feldspar in silicic rock fragments.

Table 11. Bulk analysis of basaltic lavas erupten between 1920-1930.
1. S-Botnahraun.
2. N-Botnahraun.
3. Crater on north side of Askja lake.
4. Mývetningahraun.
5. Nýjahraun.
6. Bátshraun

Table 12. Accessory minerals.

798A: Apatite in obsidian fragment.

798ol: Olivine in obsidian fragment.

799Q: Al-silicate quench products in a silicic rock fragment.

799C: Cordierite quench mineral.

TABLE 1

	V1	V2	V3	V4	V5	V6	V7	7163	7164	7165	7166	7171	798
SiO_2	65.49	66.18	69.46	67.97	70.11	68.75	68.08	69.78	69.80	69.72	69.77	69.74	70.31
Al_2O_3	12.65	13.04	12.92	12.92	13.05	13.81	13.24	13.56	13.52	13.52	13.56	13.25	13.42
TiO_2	0.98	1.00	0.86	0.91	0.91	0.98	1.04	0.89	0.90	0.89	0.92	1.00	0.97
Fe_2O_3	0.19	1.47	1.05	3.14	2.84	1.88	3.32	1.35	2.10	3.63	1.24	1.08	0.83
FeO	4.96	3.83	3.16	1.53	1.51	2.95	1.99	3.12	2.51	1.09	3.23	3.89	3.83
MnO	0.12	0.12	0.11	0.11	0.11	0.12	0.13	0.12	0.12	0.12	0.12	0.12	0.12
MgO	1.44	1.32	0.84	0.89	0.84	1.04	1.14	0.96	1.20	1.17	1.14	1.10	0.96
CaO	3.75	3.66	2.97	3.14	2.95	3.29	3.48	3.28	3.25	3.25	3.26	3.38	3.22
Na_2O	3.56	3.62	3.92	3.90	3.90	3.95	3.90	4.20	4.10	4.10	4.15	3.90	3.95
K_2O	1.96	2.00	2.20	2.21	2.23	2.12	2.08	2.09	2.09	2.09	2.09	2.14	2.20
P_2O_5													
H_2O	3.43	2.71	0.92	0.82	0.69	0.50	0.70	0.12	0.25	0.10	0.07	0.08	0.18
Total	98.53	98.95	98.41	97.54	98.91	99.39	99.10	99.47	99.84	99.68	99.55	99.68	99.99
Qz	26.04	26.28	29.77	28.25	30.27	27.45	27.07	27.75	27.83	28.91	27.72	28.54	29.02
Or	11.75	11.95	13.22	13.42	13.32	12.62	12.43	12.42	12.39	12.43	12.41	12.69	13.00
Ab	30.55	30.98	33.72	33.92	33.36	33.67	33.38	35.75	34.80	34.91	35.29	33.12	33.43
An	12.93	13.58	11.35	11.53	11.64	13.79	12.62	12.05	12.35	12.39	12.26	12.37	12.39
Di	4.10	4.04	3.09	3.80	2.68	2.25	4.10	3.66	3.22	3.23	3.37	3.77	3.04
Hy	7.10	7.25	5.26	5.37	5.30	6.73	6.47	5.49	6.39	6.28	6.06	6.34	5.98
Mt	1.26	1.26	1.00	1.09	0.10	1.12	1.22	1.05	1.06	1.06	1.06	1.18	1.10
Il	1.89	1.92	1.66	1.78	1.75	1.87	1.10	1.70	1.71	1.70	1.76	1.91	1.84
Wr	3.48	2.74	0.94	0.84	0.70	0.50	0.71	0.12	0.25	0.10	0.07	0.08	0.18
Cr	11	12	6	8	9	8	10	14	23	17	13	11	11
Ni	7	6	1	1	1		2	3	9	3	4	2	3
V	68	67	23	22	22	45	42	40	47	47	55	35	31
Cu	40	33	10	12	10	17	19	26	31	33	23	16	16
Sr	111	110	114	113	116	121	127						120
Rb	44	44	55	54	60	59	59						52
Zr	310	313	345	346	365	335	345						350
Y	59	60	73	75	78	59	58						74

TABLE 2

	V1	V2	V3	V4	V5	V7	798L (6)	798B (5)
SiO_2	70.07	70.37	71.79	72.22	72.67	72.12	72.10 ± 0.84	72.29 ± 0.98
Al_2O_3	11.90	12.08	12.13	12.33	12.22	12.34	13.35 ± 0.57	14.62 ± 0.45
TiO_2	0.84	0.80	0.76	0.84	0.86	0.96	0.85 ± 0.08	0.88 ± 0.06
FeO	4.11	3.52	3.55	3.77	3.70	4.23	3.69 ± 0.21	3.79 ± 0.22
MnO	0.14	0.07	(0.40)	0.07	0.13	0.09	0.12 ± 0.04	0.09 ± 0.04
MgO	0.73	0.67	0.72	0.77	0.70	0.81	0.96 ± 0.51	0.82 ± 0.31
CaO	2.94	2.58	2.65	2.81	2.83	2.96	2.19 ± 0.25	2.44 ± 0.24
Na_2O	2.78	3.19	3.22	3.38	3.44	3.16	3.55 ± 0.16	3.51 ± 0.18
K_2O	2.53	2.74	2.79	2.62	2.56	2.66	2.39 ± 0.06	2.26 ± 0.10
P_2O_5	0.17	0.15	0.08	0.20	0.16	0.21	0.19 ± 0.07	0.20 ± 0.05
Total	96.21	96.18	98.09	99.00	99.25	99.53	99.39	100.90
CIPW norm (Fe_2O_3/FeO = 0.15)								
Qz	36.57	34.94	35.27	34.65	35.01	34.85	34.91	34.99
Co							1.40	2.42
Or	15.53	16.83	16.87	15.63	15.23	15.78	14.20	13.23
Ab	24.44	28.05	27.88	28.87	29.31	26.85	30.21	29.42
An	13.01	10.96	10.65	10.84	10.41	11.68	9.68	10.70
Di	0.85	1.12	1.93	1.63	2.28	1.44		
Hy	6.72	5.44	5.05	5.58	5.03	6.27	6.81	6.41
Mt	0.82	0.70	0.70	0.73	0.71	0.81	0.71	0.72
Il	1.66	1.58	1.48	1.61	1.64	1.83	1.62	1.66
Ap	0.41	0.36	0.19	0.47	0.37	0.49	0.44	0.46

TABLE 3

	V1	V2	V3	798
SiO_2	49.40	50.98	48.65	49.09
Al_2O_3	13.27	13.28	12.82	13.95
TiO_2	2.07	1.87	4.38	1.78
FeO	13.27	13.13	14.74	14.32
MnO	0.22	0.22	0.25	0.18
MgO	5.96	5.96	4.87	5.82
CaO	10.91	11.06	10.10	11.05
Na_2O	2.52	2.54	2.64	2.34
K_2O	0.26	0.26	0.60	0.56
P_2O_5	0.23	0.18	0.53	0.19
Total	98.11	99.48	99.59	99.28
CIPW norm (Fe_2O_3/FeO = 0.15)				
Qz	0.55	1.74	2.01	
Or	1.56	1.54	3.55	3.33
Ab	21.70	21.57	22.39	19.91
An	24.55	24.15	21.41	26.04
Di	24.10	24.72	21.14	23.23
Hy	20.42	19.78	17.10	17.56
Ol				3.34
Mt	2.59	2.52	2.83	2.76
Il	3.10	3.56	8.34	3.40
Ap	0.54	0.42	1.23	0.44

TABLE 4

Sample	% basalt	0 bar	500 bar	1000 bar	5000 bar
V1	14	936	891	829	779
V2	14	1024	974	920	752
V3	4	1002	953	897	766
V4	6	1012	962	908	756
V5	0.4	1016	966	911	759
V6	9	1028	978	925	742
V7	12				
7163	6				
7164	7				
7165	6				
7166	6				
7174	11				

TABLE 5

	V1	V1	V2	V3	V4	V5	V7	798A	798B
SiO_2	63.93	55.87	55.62	56.49	56.81	55.90	55.63	55.22	47.75
Al_2O_3	22.76	27.34	26.57	26.34	26.34	26.67	26.71	27.91	32.82
TiO_2	0.03		0.05	0.07	0.04	0.05	0.07	0.10	0.04
FeO	0.50	0.68	0.74	0.74	0.72	0.72	0.72	0.60	0.70
MnO	0.02		0.01	0.00	0.00	0.01	0.06	0.05	0.00
MgO	0.01		0.09	0.07	0.09	0.08	0.08	0.07	0.18
CaO	4.33	9.52	10.76	10.58	10.56	10.78	11.23	10.75	16.09
Na_2O	8.42	5.61	5.44	5.52	5.63	5.53	5.28	5.91	2.34
K_2O	0.73	0.24	0.23	0.24	0.25	0.23	0.24	0.21	0.03
P_2O_5	0.00		0.03	0.02	0.01	0.00	0.00	0.00	0.03
Total	100.74	99.26	99.54	100.07	100.43	99.97	100.01	100.82	99.98
Si	11.248	10.132	10.108	10.197	10.216	10.116	10.076	9.928	8.779
Al	4.721	5.845	5.693	5.605	5.584	5.690	5.703	5.916	7.114
Ti	0.004		0.007	0.010	0.005	0.007	0.010	0.014	0.006
Fe	0.074	0.103	0.112	0.112	0.108	0.109	0.109	0.090	0.108
Mn	0.003		0.002	0	0	0.002	0.009	0.008	0
Mg	0.003		0.024	0.019	0.024	0.022	0.022	0.019	0.049
Ca	0.816	1.850	2.095	2.046	2.035	2.090	2.179	2.071	3.170
Na	2.873	1.973	1.917	1.932	1.963	1.940	1.854	2.060	0.834
K	0.164	0.056	0.053	0.055	0.057	0.053	0.055	0.048	0.007
P	0		0.001	0.001	0	0	0	0	0.001
An	21.18	47.69	51.54	50.73	50.19	51.19	53.30	49.56	79.03
Ab	74.57	50.86	47.16	47.90	48.41	47.51	45.35	49.29	20.79
Or	4.25	1.44	1.30	1.36	1.40	1.30	1.35	1.15	1.17
Z	16.05	16.08	15.92	15.92	15.91	15.92	15.90	15.95	16.01
X	3.86	3.89	4.09	4.03	4.08	4.11	4.12	4.21	4.06

TABLE 6

	V1	V2		V3		V5		V7		76B	
	cpx	cpx	opx	cpx	opx	cpx	opx	cpx	opx	cpx	opx
SiO_2	51.92	50.80	52.88	49.34	52.90	49.77	52.92	51.99	52.93	50.75	62.41
Al_2O_3	1.26	1.57	0.58	2.33	0.66	2.99	0.39	1.31	0.90	1.29	0.74
TiO_2	0.42	0.70	0.42	1.07	0.48	0.95	0.32	0.49	0.42	0.46	0.28
FeO	11.42	13.51	24.38	15.17	23.43	13.96	21.64	12.12	22.68	12.20	22.02
MnO	0.68	0.64	0.98	0.44	1.08	0.49	1.11	0.71	0.95	0.60	1.16
MgO	13.98	13.92	20.44	14.77	19.25	12.97	20.48	13.90	21.67	14.68	22.10
CaO	20.04	19.28	1.94	15.91	3.38	18.88	3.42	19.90	1.73	20.04	1.67
Na_2O	0.34	0.34	0.03	0.35	0.10	0.28	0.06	0.27	0.04	0.36	0.04
K_2O	0.00	0.01	0.03	0.01	0.05	0.01	0.04	0.01	0.00	0.02	0.00
P_2O_5	0.00	0.04	0.02	0.01	0.02	0.05	0.00	0.03	0.01	0.01	0.00
Total	100.06	100.82	101.70	99.40	101.36	100.33	100.38	100.71	101.34	100.43	100.43
Si	1.954	1.916	1.967	1.887	1.975	1.887	1.981	1.948	1.960	1.916	1.957
Al	0.056	0.070	0.025	0.105	0.029	0.134	0.017	0.058	0.039	0.057	0.033
Ti	0.012	0.020	0.012	0.031	0.013	0.027	0.009	0.014	0.012	0.013	0.008
Fe	0.359	0.426	0.759	0.485	0.732	0.443	0.677	0.380	0.702	0.385	0.688
"	0.022	0.020	0.031	0.014	0.034	0.016	0.035	0.023	0.030	0.019	0.037
Mg	0.784	0.782	1.133	0.842	1.071	0.733	1.142	0.776	1.196	0.826	1.230
Ca	0.808	0.779	0.077	0.652	0.135	0.767	0.137	0.799	0.069	0.811	0.067
Na	0.025	0.025	0.002	0.026	0.007	0.021	0.004	0.020	0.003	0.026	0.003
K	0	0	0.001	0	0.002	0	0.002	0	0	0.001	0
D	0	0.001	0.001	0	0.001	0.002	0	0.001	0	0	0
Ca	41.0	38.8	3.9	32.7	6.8	39.2	6.9	40.4	3.5	39.7	3.3
Mg	39.7	39.0	56.7	42.2	54.3	37.4	57.4	39.2	59.9	40.5	60.8
Fe	19.3	22.2	39.5	25.0	38.8	23.4	35.8	20.4	36.7	19.8	35.9

TABLE 7

Sample	V2				V3				V4				V5				V7			
	spin.		rhomb.		spin.		rhomb.		spin.		rhomb.		spin.		rhomb.		spin.		rhomb.	
	(3) x	s	(4) x	s	(6) x	s	(4) x	s	(4) x	s	(4) x	s	(5) x	s	(8) x	s	(6) x	s	(5) x	s
SiO_2	0.10	0.02	0.02	0.02	0.11	0.01	0.04	0.02	0.12	0.02	0.04		0.09	0.03	0.13	0.16	0.15	0.04	0.04	0.01
TiO_2	13.38	0.81	41.76	0.86	14.64	0.83	42.00	0.28	12.09	3.25	42.21	0.60	14.10	2.18	42.66	1.33	12.62	5.90	42.46	2.17
Al_2O_3	2.87	0.10	0.39	0.01	2.71	0.06	0.42	0.02	2.73	0.56	0.45	0.02	2.90	0.54	0.43	0.08	3.22	1.30	0.48	0.04
Cr_2O_3	0.00		0.02	0.02	0.02	0.02	0.00		0.00		0.02	0.03	0.03	0.03	0.01	0.01	0.01	0.02		
V_2O_3	0.19	0.02	0.27	0.04	0.21	0.05	0.25	0.03	0.26	0.03	0.33	0.03	0.38	0.19	0.40	0.07	0.32	0.09	0.35	0.07
Fe_2O_3	41.00		21.65		39.04		21.76		44.34		21.95		39.51		20.69		42.99		51.51	
FeO	39.95	1.24	31.31	0.34	41.18	0.76	31.47	0.40	38.98	3.33	31.34	0.10	40.91	2.35	32.01	1.03	39.87	5.40	32.77	2.57
MnO	0.63	0.05	0.71	0.02	0.65	0.06	0.62	0.03	0.68	0.04	0.64	0.01	0.62	0.04	0.63	0.05	0.59	0.29	0.43	0.08
NiO	0.00		0.04	0.06	0.06	0.04	0.01	0.03	0.03	0.04	0.00		0.03	0.03	0.01	0.02			0.03	0.04
MgO	2.26	0.14	3.02	0.12	2.32	0.06	3.11	0.06	2.31	0.24	3.26	0.09	2.20	0.12	3.22	0.23	2.40	0.47	2.69	0.38
CaO	0.03	0.03	0.05	0.05	0.03	0.02	0.09	0.04	0.02	0.02	0.14	0.16	0.02	0.02	0.02	0.03	0.03	0.03	0.03	0.03
ZnO	0.23	0.03	0.06	0.10	0.12	0.06	0.05	0.05	0.21	0.07	0.03	0.04	0.08	0.13	0.14	0.16	0.04	0.06	0.18	0.09
Total	100.65		99.30		101.09		99.82		101.77		100.40		100.88		100.31		102.25		100.97	
Usp	41.8				45.2				37.7				43.8				39.5			
Mt	65.1				52.5				59.1				54.1				58.5			
Ilm			76.11				76.13				75.84				77.17				76.10	
Hem			23.89				23.87				24.16				22.83				23.00	

TABLE 8

	1307	800	1200	AFR	799	1305	797	794	793	792
SiO_2	73.43	72.97	78.60	80.64	77.80	71.91	77.81	72.69	71.49	69.97
Al_2O_3	12.57	13.68	11.46	10.55	12.67	11.86	12.48	12.90	12.97	13.26
TiO_2	0.48	0.18	0.19	0.18	0.19	0.17	0.21	0.30	0.50	0.84
Fe_2O_3	1.75	1.97	1.75	0.21	0.70	5.19	1.38	3.72	2.65	2.73
FeO	1.89	0.00	0.00	0.96	0.00	1.46	0.48	1.08	1.68	1.48
MnO	0.08	0.03	0.02	0.02	0.01	0.02	0.02	0.07	0.10	0.12
MgO	0.54	0.03	0.03	0.18	0.02	0.04	0.10	0.14	0.41	0.85
CaO	1.99	1.18	0.89	1.20	1.14	0.69	1.13	2.13	2.41	2.91
Na_2O	3.81	4.65	3.60	3.30	4.40	4.05	3.00	4.13	4.20	4.30
K_2O	2.36	3.33	2.76	1.75	2.03	2.05	2.59	2.40	2.33	1.91
P_2O_5										
H_2O	0.25	0.67	0.37	0.48	0.35	1.51	0.76	0.13	0.42	0.58
Total	99.15	98.69	99.67	99.47	99.31	98.95	99.96	99.69	99.16	98.95
δO^{18} o/oo	-4.7	-7.4	-7.2		-9.9			-5.2	-4.8	(0-1)
Qz	35.55	30.01	44.46	51.55	42.00	35.63	46.98	32.42	30.85	29.18
Co	0.13	0.28	0.94	1.05	1.17	1.75	2.69			
Or	14.08	19.97	16.39	10.40	12.09	12.29	15.33	14.27	13.91	11.43
Ab	32.55	39.93	30.61	28.07	37.51	34.78	25.42	35.16	35.91	36.85
An	9.97	5.94	4.44	5.98	5.70	3.47	5.61	9.63	9.76	11.38
Di								0.88	2.02	2.75
Hy	5.69	2.39	2.05	1.84	0.66	8.71	2.38	5.85	5.17	5.25
Mt	0.85	0.44	0.38	0.28	0.16	1.50	0.42	1.08	0.10	0.97
Il	0.92	0.35	0.36	0.34	0.36	0.33	0.40	0.57	0.96	1.62
Wr	0.25	0.68	0.37	0.48	0.35	1.53	0.76	0.13	0.42	0.59
Cr	6	3	5	2	2	15	8	7	9	
Ni	2				3	2	3			
V	27		3	2	2	2	2	3	4	29
Cu	44	9	4		2	75		12	9	11
Sr	90	42	72		88	70	73		96	115
Rb	52	78	70		20	58	72		64	47
Zr	360	380	320		380	260	480		390	490
Y	115	240	120		61	48	102		49	76

TABLE 9

	794A	794B	799	800
SiO_2	75.45	72.30	78.53	74.59
Al_2O_3	13.68	12.87	12.32	14.89
TiO_2	0.21	0.55	0.18	0.28
FeO	1.19	2.61	0.43	0.88
MnO	0.11	0.14	0.02	0.03
MgO	0.03	0.30	0.10	0.36
CaO	0.55	1.03	0.34	0.33
Na_2O	3.85	4.12	2.70	3.54
K_2O	5.20	4.70	4.76	4.44
P_2O_5	0.06	0.01	0.01	0.05
Total	100.33	98.62	99.41	99.39
CIPW norm ($Fe_2O_3/FeO = 0.15$)				
Qz	31.24	27.08	43.85	35.70
Co	0.86		2.14	3.80
Or	30.62	28.15	28.30	26.40
Ab	32.47	35.33	22.99	30.13
An	2.33	2.78	1.63	1.32
Di		2.02		
Hy	1.72	3.05	0.64	1.83
Mt	0.23	0.51	0.08	0.17
Il	0.40	1.06	0.34	0.53
Ap	0.14	0.02	0.02	0.12

TABLE 10

	799		794		800	
	A	B	C	R	A	B
SiO_2	60.76	67.23	57.73	64.22	63.74	65.64
Al_2O_3	23.63	20.35	25.13	21.10	22.02	21.39
TiO_2	0.07	0.08				
FeO	0.11	0.14	0.33	0.29	0.38	0.39
MnO	0.01	0.02				
MgO	0.01	0.05				
CaO	6.79	5.07	7.50	3.00	4.68	4.52
Na_2O	7.06	4.48	7.20	7.78	8.29	7.36
K_2O	1.05	1.86	0.92	2.74	1.19	1.62
P_2O_5	0	0.02				
Total	99.48	99.30	98.82	99.13	100.31	100.92
Si	10.904	11.835	10.510	11.513	11.297	11.513
Al	4.999	4.223	5.393	4.459	4.601	4.423
Ti	0.009	0.011				
Fe	0.017	0.021	0.050	0.043	0.056	0.057
Mn	0.002	0.003				
Mg	0.003	0.013				
Ca	1.306	0.956	1.463	0.576	0.889	0.849
Na	2.457	1.529	2.542	2.704	2.849	2.503
K	0.240	0.418	0.214	0.627	0.269	0.363
P	0	0.001				
An	32.63	32.93	34.68	14.74	22.19	22.85
	61.38	52.67	60.25	69.21	71.10	67.38
Or	5.99	14.40	5.07	16.05	6.71	9.77

TABLE 11

Sample	1	2	3	4	5	6
SiO_2	50.70	51.20	50.87	50.44	50.24	50.87
TiO_2	2.64	2.80	2.57	2.72	2.65	2.95
Al_2O_3	13.06	13.31	13.59	13.07	14.03	12.92
Fe_2O_3	5.24	4.93	7.61	4.67	2.29	2.85
FeO	10.88	11.16	8.48	11.40	13.33	13.19
CaO	8.64	8.36	8.72	8.58	8.50	9.02
MgO	4.82	4.52	4.79	4.93	4.93	5.40
MnO	0.25	0.23	0.22	0.22	0.28	0.26
P_2O_5	0.26	0.26	0.26	0.26	0.28	
Na_2O	2.32	2.50	2.38	2.40	2.68	2.46
K_2O	0.69	0.76	0.74	0.69	0.58	0.76
H_2O^+	0.24	0.20	0.09	0.69	0.20	0.17
H_2O^-	0.20	0.25	0.13	0.19	0.12	0.04
Total	99.94	100.48	100.45	100.26	100.11	100.89

TABLE 12

	798A	798ol	799Q		799C
SiO_2	0.41	36.47	32.93	34.85	48.90
Al_2O_3	0.00	0.05	52.96	64.47	31.95
TiO_2	0.04	0.10	0.75	0.51	0.00
FeO	0.53	32.40	1.40	0.51	3.91
MnO	0.12	0.51	0.00	0.03	0.16
MgO	0.27	32.55	0.38	0.18	11.76
CaO	51.11	0.38	0.00	0.00	0.06
Na_2O	0.08	0.01	0.13	0.12	0.07
K_2O	0.04	0.03	0.00	0.01	0.10
P_2O_5	39.26	0.08	0.00	0.05	0.00
Total	91.85	102.59	88.54	100.73	96.91